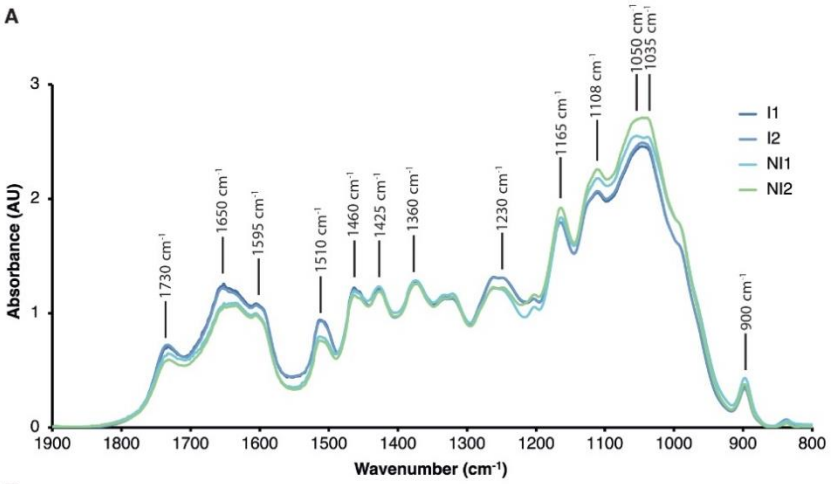

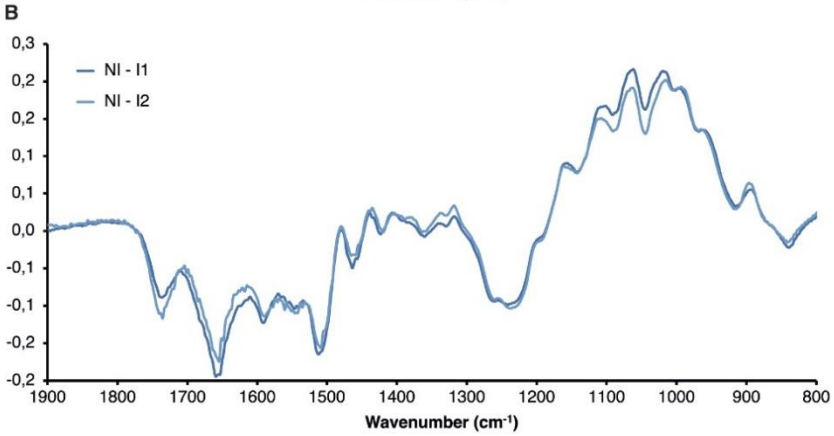

C

Compound	NI	I
Acetyl/lignins (1,730 cm^{-1} / 1,510 cm^{-1})	0.80 ± 0.02	0.76 ± 0.01
Cellulose/lignins (1,100 cm^{-1} / 1,510 cm^{-1})	2.9 ± 0.16	2.2 ± 0.03

D

Wavenumber (cm^{-1})	Attribution
990	C6–O6H stretching (cellulose) C–O stretching or –CH=CH– out of plane bending (lignin)
1,035	C=O stretching (cellulose, hemicellulose, lignin)
1,050	C–O stretching from C3–O3H secondary alcohol
1,108	Asymmetric in-phase ring stretching, C–C and C–CO stretching, ring asymmetric valence vibration secondary alcohol group, C–O stretching (cellulose)
1,165	Asymmetric C–O–C stretching vibration (cellulose)
1,230	OH plane deformation (cellulose, hemicellulose)
1,360	C–H bending (cellulose)
1,425	C–OH bending vibration of C2–OH groups
1,460	CH2 symmetric bending on xylose rings
1,510	C=C aromatic skeleton vibrations
1,595	C=C aromatic skeleton vibrations
1,650	C=O stretching
1,730	C=O stretching vibration in COOH groups of glucuronic units of xylan

Supplementary Figure 1: Impact of wild type *R. cellulolyticum* growth on hatched wheat straw (WS). A. Fourier Transform InfraRed spectroscopy (FTIR) spectra acquired on residual substrates after anaerobic *R. cellulolyticum* growth (I1 and I2) and on uninoculated control incubated in the same conditions (NI1 and NI2). A baseline correction considering the 4000 to 400 cm^{-1} spectral range and a normalization considering the 1900 to 800 cm^{-1} spectral range were applied on the presented spectra. Samples preparation is described in the Material and Methods section "Fourier transform InfraRed (IR) spectroscopy of whole plant cell wall". **B.** Difference between the mean NI spectrum (mean curve of NI1 and NI2 spectra) and I1 or I2 spectra depicted in **A. C**. Intensity

ratio of bands associated with hemicellulose (acetyl, 1730 cm^{-1}), cellulose (1110 cm^{-1}) and lignin (1510 cm^{-1}) (mean and standard deviation calculated from duplicates). **D.** Attribution of the IR signals depicted in **A.**.

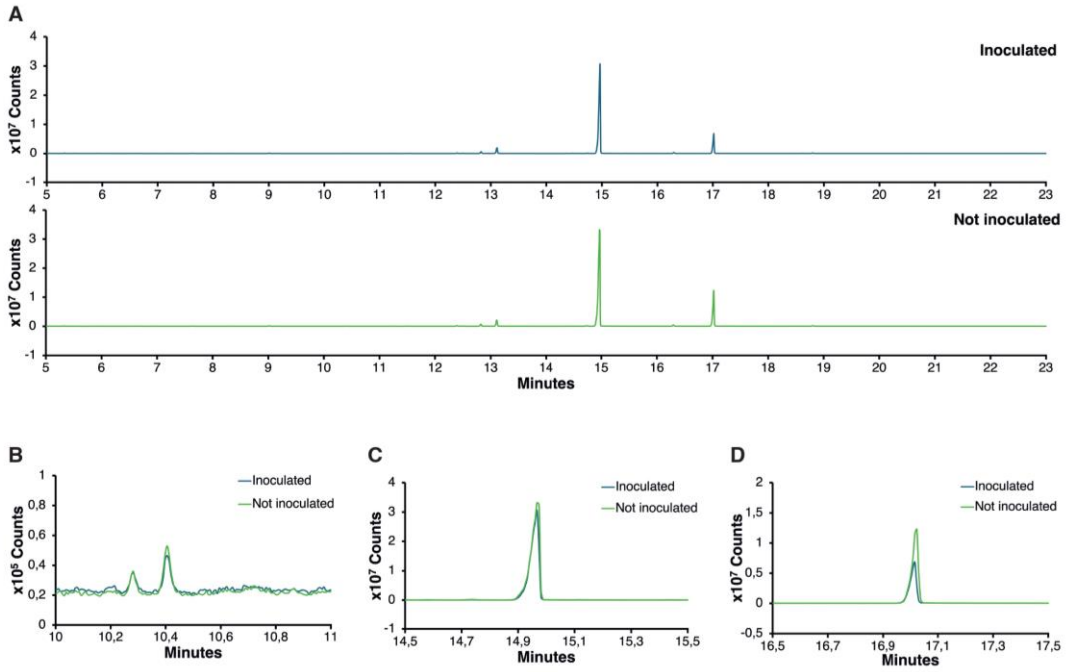

Supplementary Figure 2: GC-MS analysis of the post-alkali hydrolysis extractives of the residual insoluble WS after *R. cellulolyticum* anaerobic growth. A. Example of full-scale GC-MS chromatograms of the products of the alkaline hydrolysis of the residual insoluble WS after anaerobic *R. cellulolyticum* growth (Inoculated) and of an uninoculated control incubated in the same conditions (Not inoculated). **B.** Zoom of **A.** in the retention time range 10 to 11 min where 4-OH benzoic acid (4-OH-B) should be detected. **C.** Zoom of **A.** in the retention time range 14.5 to 15.5 min where *p*-coumaric acid (*p*CA) should be detected. **D.** Zoom of **A.** in the retention time range 16.5 to 17.5 min where the ferulic acid (FA) should be detected. A decrease of the ratio between the FA and pCA quantities is observable in the "Inoculated" condition compared to the control (Not inoculated). The experiments were performed on biological triplicates and display the same phenomenon.

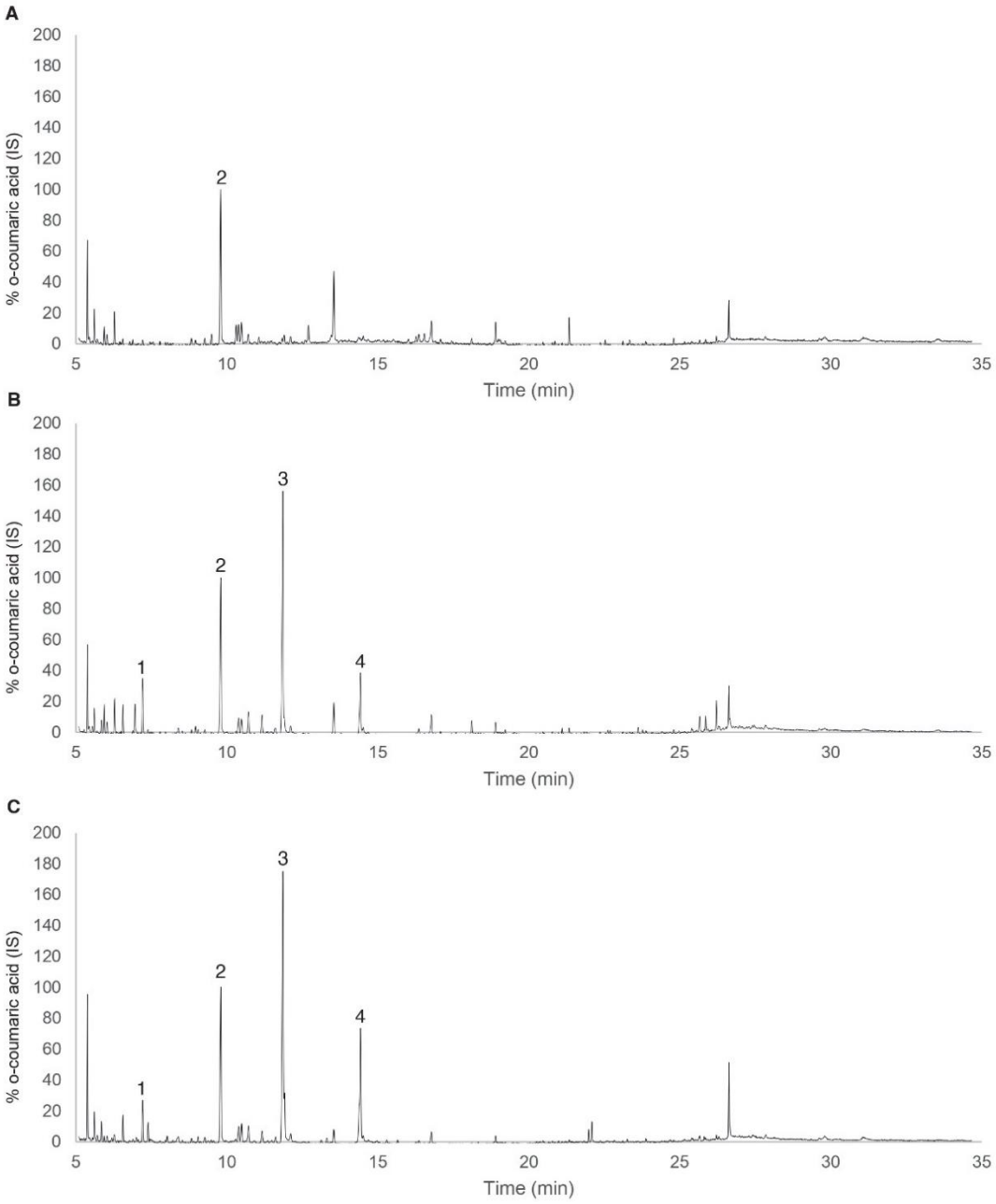

Supplementary Figure 3: GC-MS compositional analysis chromatograms of lyophilized culture supernatants after anaerobic growth on WS of wild type *R. cellulolyticum* and of the strain pSOS-2017 overproducing the truncated form (without dockerin) of SGNHh$_{2017}$ (SGNHh$_{2017}$*). Examples of GC-MS chromatograms of extractives from lyophilized culture supernatants after anaerobic growth of wild type (**B.**) and SGNHh$_{2017}$* overproducing (**C.**) *R. cellulolyticum* strains on WS and of uninoculated control incubated in the same conditions (**A.**). The chromatograms are normalized according to the peak area attributed to the internal standard (o-coumaric acid, peak 2 area = 100 %). Samples preparation is described in the Material and Methods section "GC-MS compositional analysis of *R. cellulolyticum* culture supernatant and post alkali hydrolysis of the washed residual WS". Peak allocation: 4-OH benzoic acid (1, 4-OH-B), the o-coumaric acid (2) used as internal standard, the *p*-coumaric acid (3, *p*CA) and the ferulic acid (4, FA).

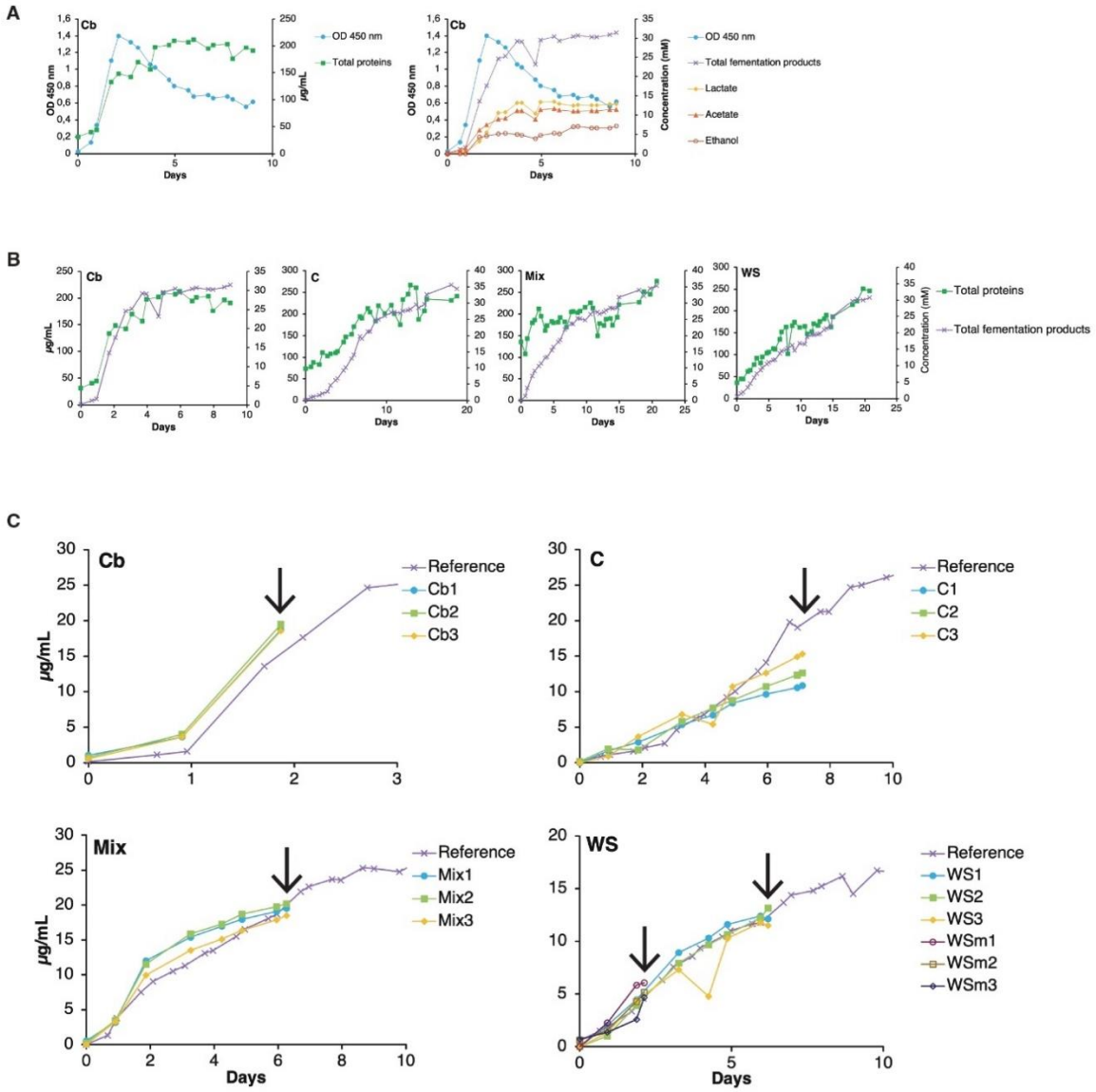

Supplementary Figure 4: *R. cellulolyticum* anaerobic growth on cellobiose (Cb), crystalline cellulose (C), Mix of selected polysaccharides (Mix) and hatched wheat straw (WS) monitored *via* metabolic profiling (MP) and sampling times for the transcriptomic analysis. A. Examples of growth monitoring of *R. cellulolyticum* on Cb, comparing the optical density measurement at 450 nm (OD_{450}, blue dots) either with the determination of the total protein concentration (Lowry assay, green squares, left panel) or with MP (Total fermentation products (lactate + acetate + ethanol) in purple crosses, lactate in orange diamonds, acetate in red triangles and ethanol in red circle, right panel). MP seems to be more reliable than the Lowry quantification compared to the OD_{450} measurement and was then used to follow the bacterial growth to overcome the limitations associated with the C, Mix and WS insoluble nature, that hampers standard spectrophotometric technique use. **B.** Examples of *R. cellulolyticum* anaerobic growth on Cb, C, Mix and WS monitored by determination of the total protein concentration (Lowry assay, green squares) and by MP (Total fermentation products, purple crosses) confirming the reliability of MP to follow *R. cellulolyticum* growth on insoluble substrates (C, Mix and WS). **C.** Each panel depicts the growth curves of *R. cellulolyticum* followed by MP (performed in triplicates) using Cb (Cb1-3), C (C1-3), Mix (M1-3) and WS (WS1-3 and WSm-1-3) in comparison with the corresponding reference growth curve (purple crosses) depicted in **B.** The growth curves corresponding to first, second and third biological replicates 1, 2 and 3 are shown in light blue full circles, light green squares, and yellow diamonds, respectively. The curves corresponding to the replicates WSm1, 2 and 3 are shown using maroon empty circles, khaki empty squares and marine blue empty diamonds respectively. Cb1-3, C1-3, M1-3 and WS1-3 samplings (vertical black arrows) were performed at the end-exponential phases of the growth whereas WSm-1-3 sampling was performed at the mid-exponential phases of the growth on WS.

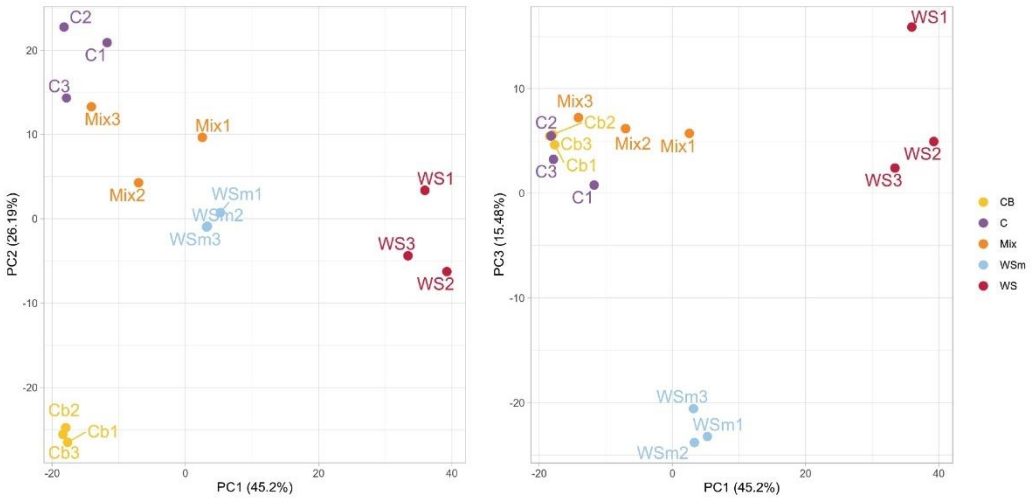

Supplementary Figure 5: Principal component analysis (PCA) of RNAseq data. Each dot represents a biological replicate of RNA-Seq samples obtained after growth of *R. cellulolyticum* on cellobiose (Cb1-3), crystalline cellulose (C1-3), Mix of selected polysaccharides (M1-3) and hatched wheat straw (WS1-3 and WSm1-3) described in Supplementary Fig. 4. The scatterplots presented here explain the majority of the information given by the data (86,87 %). The first plot (left panel) indicates a high level of similarity among the biological replicates and the first dimension shows a good separation between the samples obtained from growth on polysaccharides (Cb, C and Mix) and WS, whereas the second dimension allows to discriminate the Cb conditions from the C and Mix ones. The closeness between C and Mix could be corelated to the presence of crystalline cellulose in the Mix of selected polysaccharides used in this study. With respect to the Wsm condition, it seems to be intermediate between the samples obtained from growth on polysaccharides (Cb, C and Mix) and WS. This could be explained by *R. cellulolyticum* biological activity that both consumes the polysaccharidic fraction and modifies the lignin of the WS, meaning that the composition of this growth substrate evolves all along the bacterial growth. Consequently, this compositional difference will therefore be more marked between the mid- (Wsm) and the end- (WS) exponential growth phases for the latter, more sugar being present in the Wsm condition compared to the WS one. However, in the second plot (right panel), the third dimension demonstrates a clear and strong difference between WS and WSm samples.

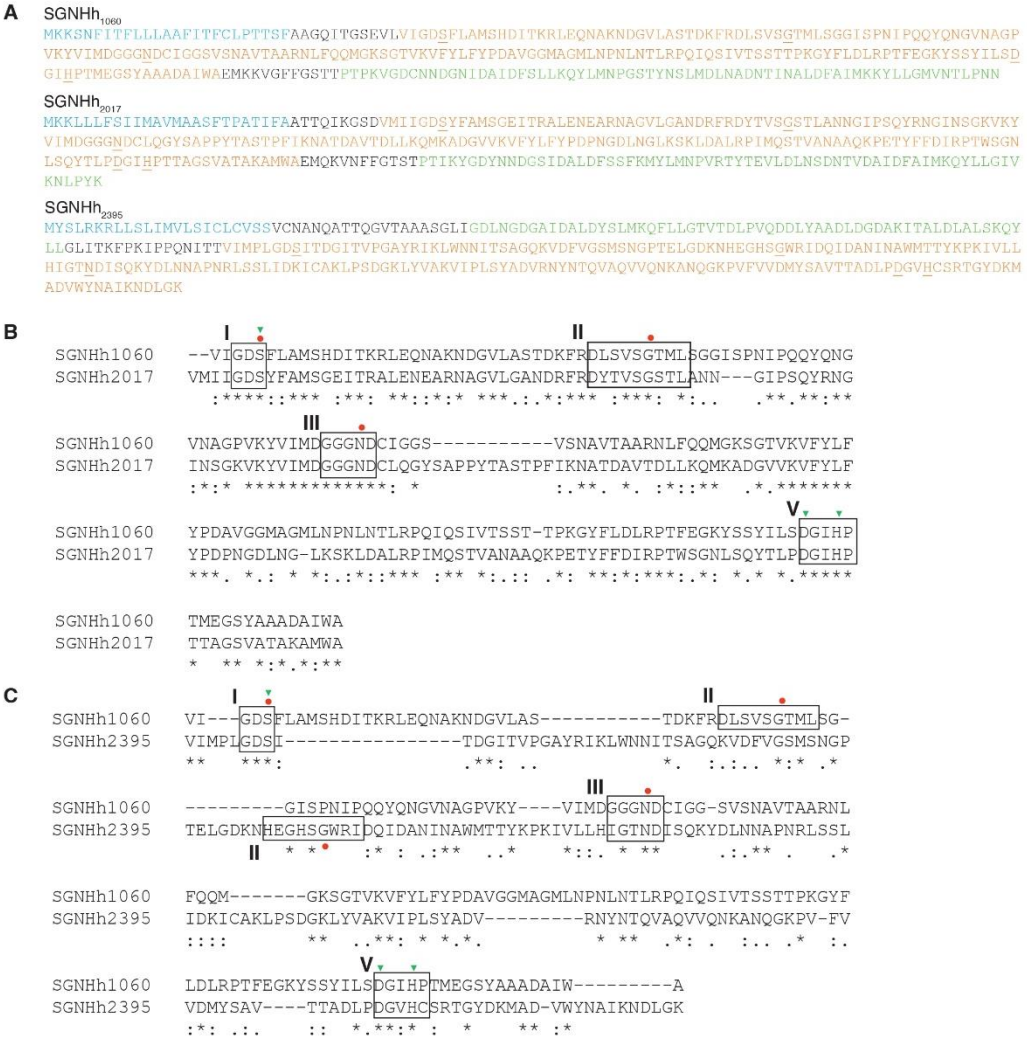

Supplementary Figure 6: SGNHh$_{1060}$, SGNHh$_{2017}$ and SGNHh$_{2395}$ catalytic domain amino-acid sequences comparison. A. Aminoacid sequences of the full size SGNHh$_{1060}$, SGNHh$_{2017}$ and SGNHh$_{2395}$ proteins. The sequences of the signal peptide, the SGNHh catalytic domain and the dockerin domain are in blue, orange and green respectively. **B.** Sequence alignment of the SGNHh$_{1060}$ and SGNHh$_{2017}$ catalytic domains generated using MAFFT[128]. **C.** Sequence alignment of the SGNHh$_{1060}$ and SGNHh$_{2395}$ catalytic domains generated using MAFFT[128]. In **B.** and **C.**, the blocks I, II, III and V containing the conserved catalytic triad (labelled with a green triangle) and the residues implicated in the oxyanion hole formation (labelled with a red circle) are boxed. (*), (:) and (.) symbols correspond with positions with a single and fully conserved residue, with conservation between amino acid groups of similar properties and with conservation between amino acid groups of weakly similar properties, respectively.

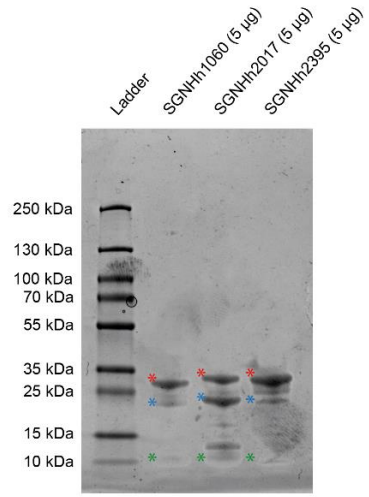

Supplementary Figure 7: Coomassie blue stained SDS PAGE analysis of the three purified recombinant SGNHhs (SGNHh$_{1060}$, SGNHh$_{2017}$ or SGNHh$_{2395}$). 5 µg of purified recombinant SGNHh$_{1060}$, SGNHh$_{2017}$ and SGNHh$_{2395}$ were analyzed by SDS-PAGE and Coomassie blue stained. They were loaded in lanes marked SGNHh1060(5 µg), SGNHh2017(5 µg) and SGNHh2395(5 µg) respectively. The ladder was loaded in the first gel lane (the corresponding molecular weights are indicated on the left of each gel). A band was detected for SGNHh$_{1060}$, SGNHh$_{2017}$ and SGNHh$_{2395}$ at the expected molecular weights (red *) whereas additional bands are mainly observed for SGNHh$_{2017}$ whose molecular weights correspond to the one of the form without dockerin (blue *) and of the cleaved dockerin (green *) respectively. The cleavage of the linker between dockerin and the catalytic domain of cellulases from *R. cellulolyticum* is a known phenomenon occurring during the purification of cellulosomal enzymes heterologously produced in *E. coli*. This gel demonstrates that the three recombinant SGNHh heterologously produced in *E. coli* were purified to homogeneity avoiding any contamination by *E. coli*'s cytoplasmic esterases that would have interfered with the activity measurements described in Figure 3.

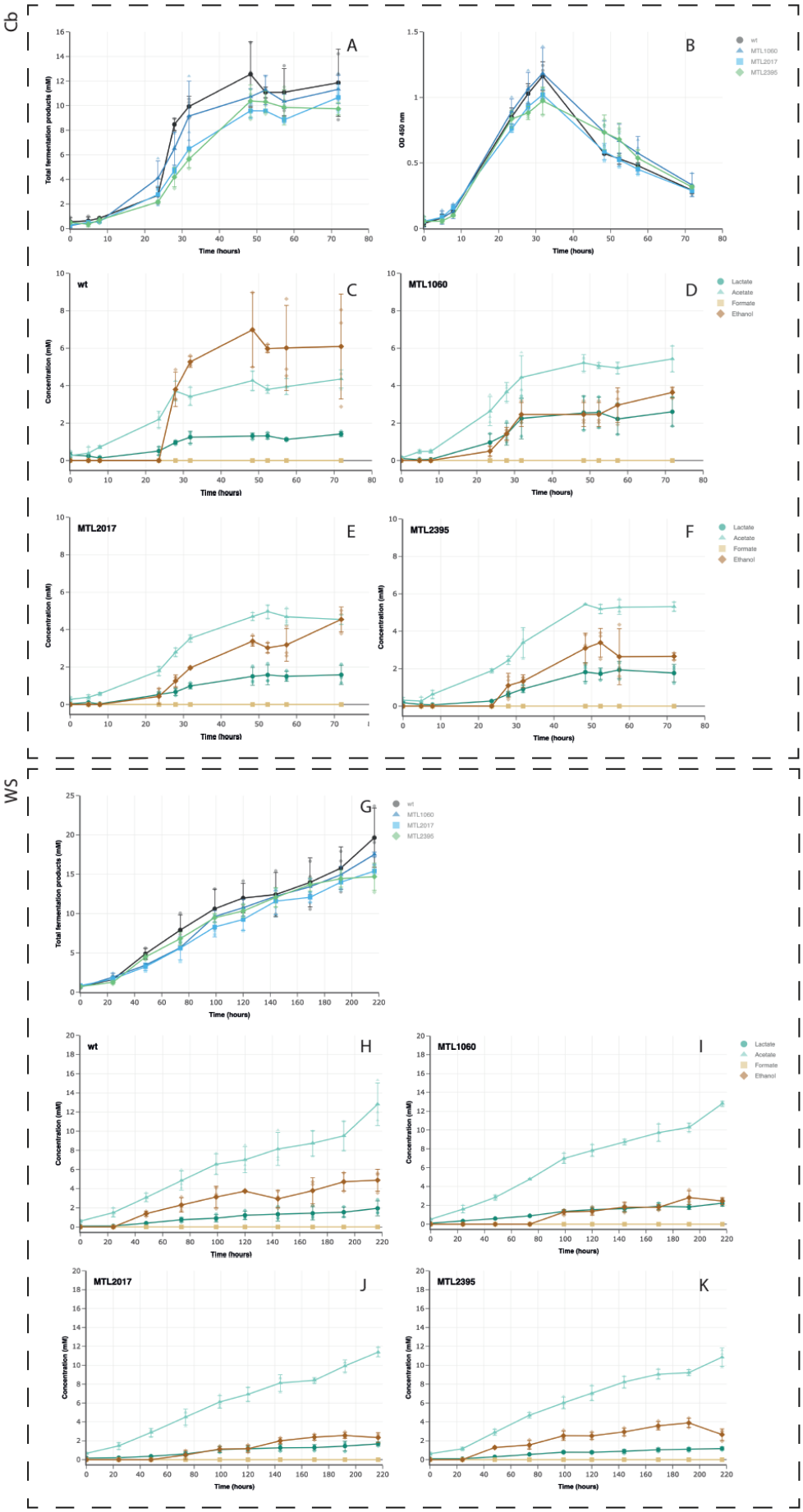
Cb
A
B
C
D
E
F
WS
G
H
I
J
K
wt
MTL1060
MTL2017
MTL2395
Lactate
Acetate
Formate
Ethanol
Total fermentation products (mM)
OD 650 nm
Concentration (mM)
Time (hours)

94

Supplementary Figure 8: Effect of the single inactivation of the genes coding for $SGNHh_{1060}$, $SGNHh_{2017}$ or $SGNHh_{2395}$ in of wild type *R. cellulolyticum* during anaerobic growth on cellobiose (Cb) and WS. The single inactivation of the isolated $SGNHh_{1060}$, $SGNHh_{2017}$ and $SGNHh_{2395}$ encoding genes generated the strains MTL1060, MTL2017 and MTL2395, respectively. The anaerobic growth of the various strains on Cb (**A.** to **F.**) and WS (**G.** to **K.**) were performed at 32°C and followed *via* MP (see legend of Supplementary Fig. 4 for details on MP). The subsequent evolution over time of the concentration of the total fermentation products excreted (Sum [lactate + acetate + ethanol + formate]) in the culture supernatants for all strains are depicted in **A.** and **G.** The evolution of the concentration of lactate, acetate, ethanol and formate for each strain is detailed in **C.** to **F.** and **H.** to **K.**. **B.** Growth of the various strains on Cb monitored by optical density measurement at 450nm (OD_{450}) whose comparison with **A.** confirms that MP seems to be as reliable to follow the growth (see legend of the Supplementary Fig. 4). All experiments were carried out in triplicates and the mean and standard deviation are presented. All error bars presented are standard errors of the mean.

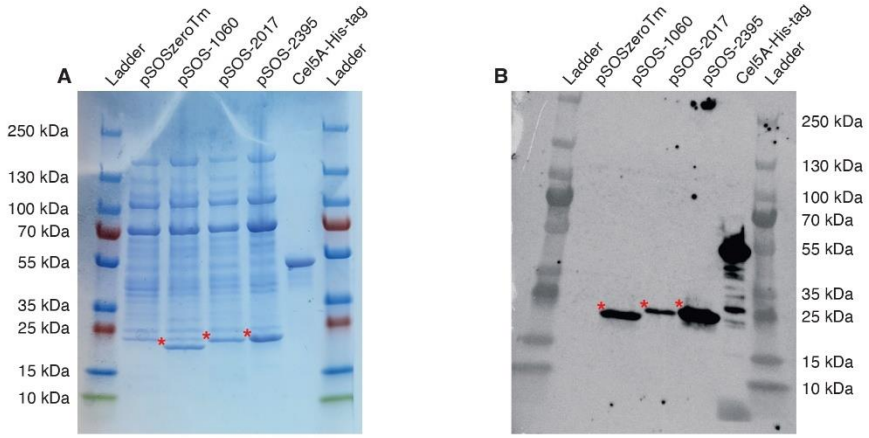

Supplementary Figure 9: Secretome analysis of the SGNHh$_{1060}$*, SGNHh$_{2017}$* or SGNHh$_{2395}$* overproducing *R. cellulolyticum* strains grown on cellobiose (Cb). The culture supernatants of wild type *R. cellulolyticum* strains transformed with the plasmids pSOS-1060, pSOS-2017, pSOS-2395 (allowing the overproduction of SGNHh$_{1060}$*, SGNHh$_{2017}$* or SGNHh$_{2395}$* respectively) and pSOSzeroTm (control strain), were collected at the end exponential phase of the growth on Cb at 32°C. The resulting TCA precipitated proteins were analyzed by SDS-PAGE and Coomassie blue stained (**A.**) or detected by Immunoblotting using an antibody anti His-tag (**B.**). The protein Cel5A with a His-tag was used as a control (Cel5A-His-tag lane) for the Immunoblot. The ladder was loaded in the first gel lane (the corresponding molecular weights are indicated on the left of each gel). The additional bands detected for the overexpressing strain (red * in pSOS-1060, pSOS-2017 and pSOS-2395 lanes) compared to the control strain are at the expected molecular weight for each overexpressed protein (**A.**) and are detected on the immunoblot (**B.**) demonstrating that SGNHh$_{1060}$*, SGNHh$_{2017}$* or SGNHh$_{2395}$* are efficiently secreted in each engineered strain.

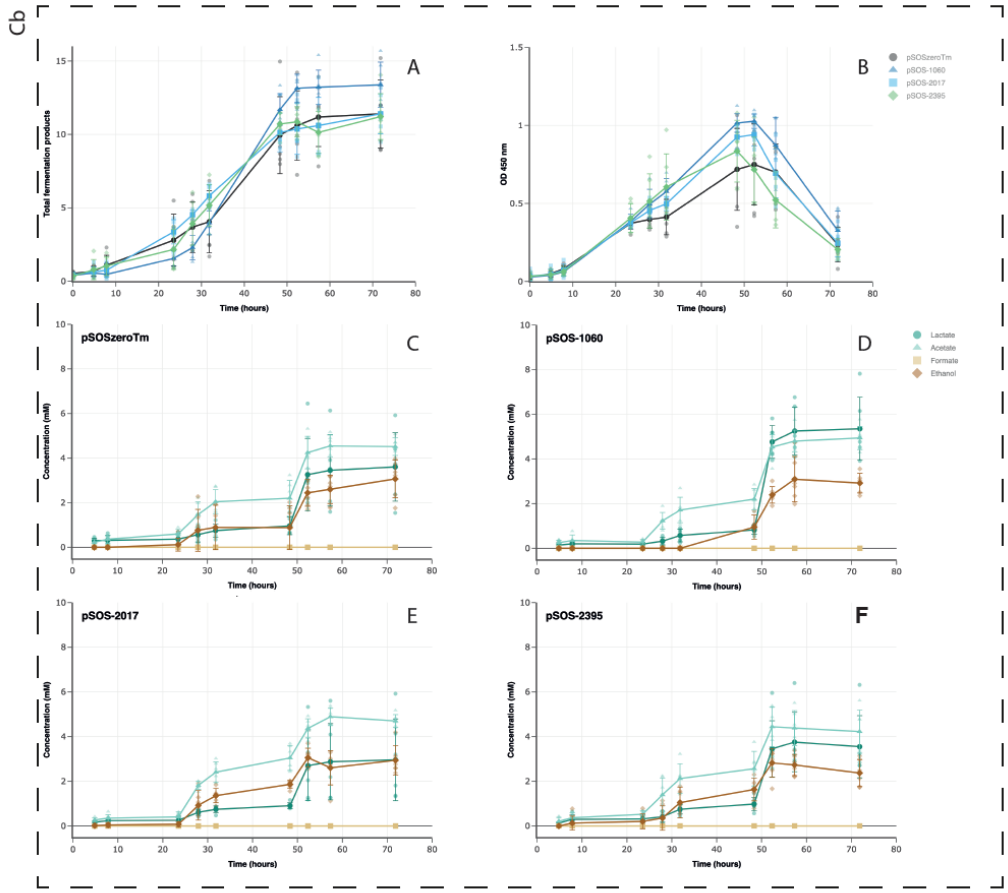
Cb
A
B
C
D
E
F
Total fermentation products
OD 450 nm
Concentration (mM)
Time (hours)
pSOSzeroTm
pSOS-1060
pSOS-2017
pSOS-2395
Lactate
Acetate
Formate
Ethanol

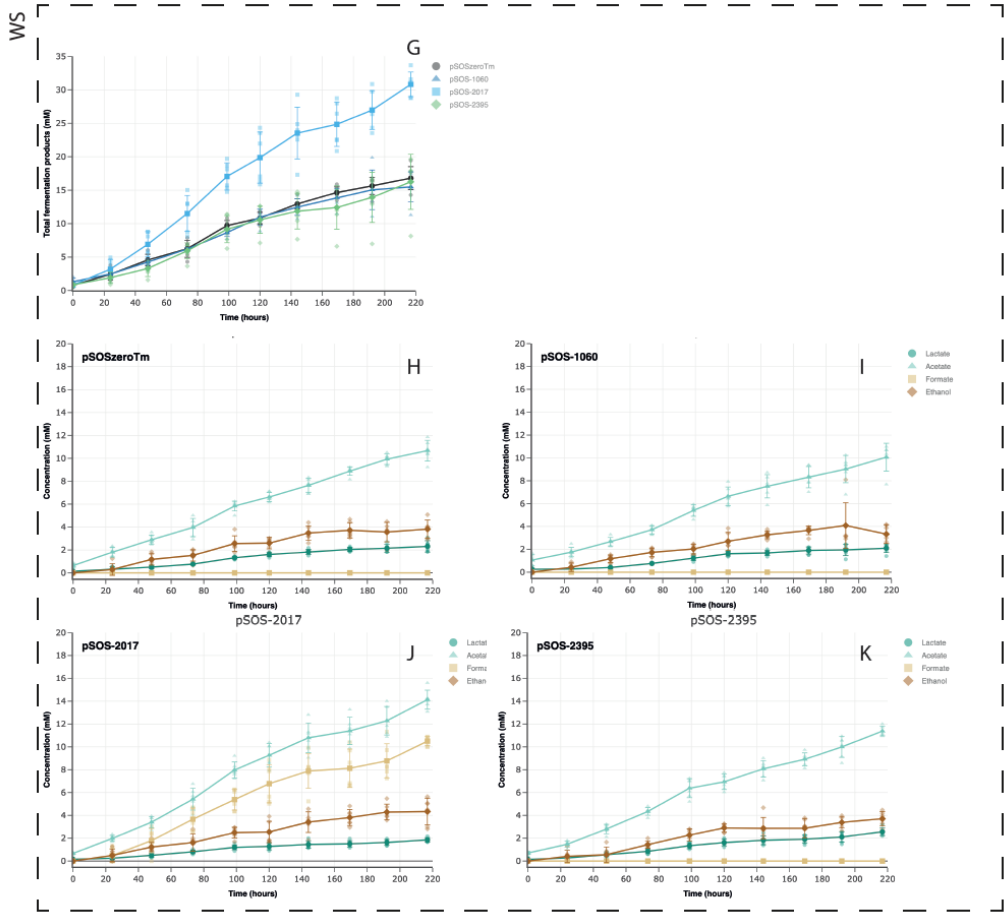
WS
G
H
I
J
K
Total fermentation products (mM)
Concentration (mM)
Time (hours)
pSOSzeroTm
pSOS-1060
pSOS-2017
pSOS-2395
Lactate
Acetate
Formate
Ethanol

120

Supplementary Figure 10: Growth curves of control and SGNHh$_{1060}$*, SGNHh$_{2017}$* or SGNHh$_{2395}$* overproducing *R. cellulolyticum* strains on cellobiose (Cb) and hatched wheat straw (WS). The anaerobic growth on Cb (**A.** to **F.**) and WS (**G.** to **K.**) were performed at 32°C and followed *via* MP (see legend of Supplementary Fig. 4 for detail of MP). The subsequent evolution over time of the concentration of the total fermentation products excreted (Sum [lactate + acetate + ethanol + formate]) in the culture supernatants for all strains are depicted in **A.** and **G.** The evolution of the concentration of lactate, acetate, ethanol and formate for each strain is detailed in **C.** to **F.** and **H.** to **K.**. **B.** Growth of the various strains on cellobiose monitored by optic density measurement at 450nm (OD_{450}) whose comparison with **A.** confirms that MP seems to be as reliable to follow the growth (see legend of the Supplementary Fig. 4). All experiments were carried out in triplicates and the mean and standard deviation are presented. All error bars presented are standard errors of the mean.

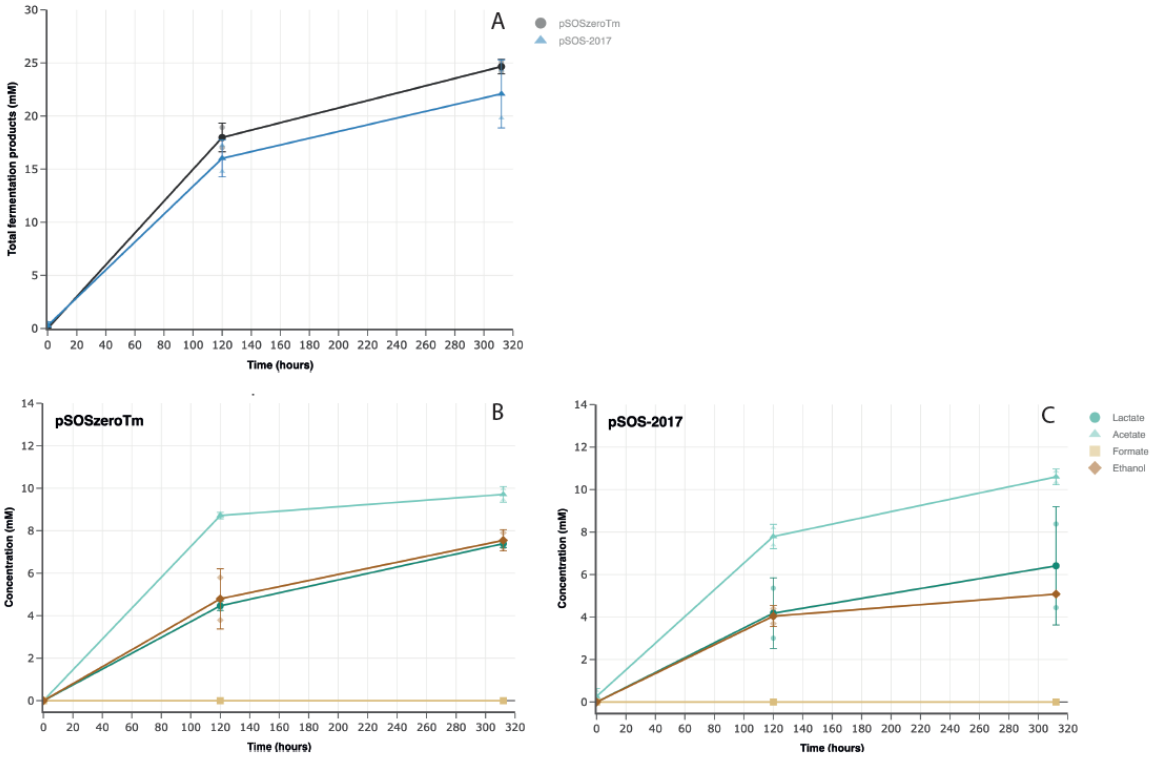

Supplementary Figure 11: Growth of SGNHh$_{2017}$* overproducing *R. cellulolyticum* strain on Mix. The anaerobic growth on Mix of wild type *R. cellulolyticum* strains transformed with the plasmids pSOS-2017 (allowing the overproduction of SGNHh$_{2017}$*) and pSOSzeroTm (control strain) were performed at 32°C and followed *via* MP (see legend of Supplementary Fig. 4 for detail of MP). The evolution of the concentration of the total fermentation products excreted (Sum [lactate + acetate + ethanol + formate]) for both (**A.**) and the detailed evolution of the concentration of the lactate, acetate, ethanol and formate concentrations for pSOSzeroTm (**B.**) and pSOS-2017 (**C.**) transformed strains are detailed. The experiments were carried out in triplicates and the mean and standard deviation are presented. All error bars presented are standard errors of the mean.

Supplementary table 1: Primers used in this study.

Name	Sequence	Comments
Ccel_1060-NcoI-F	GGGGGCCATGGCCGGCCAAATTACAGGAAG	Construction of the plasmids for *E. coli* production in
Ccel_1060-XhoI-R	GGGGGCTCGAGGTTATTTGGTAATGTATTTACCATTCCAAG	
Ccel_2395-NcoI-F	TACCCATGGCATGTAATGCTAACCAG	
Ccel_2395-XhoI-R	GTGCTCGAGTTTGCCTAAATCATTTTTGATAGC	
1060-EBS1d	CAGATTGTACAAATGTGGTGATAACAGATAAGTCCAGTTCCATAACTTACCTTTCTTTGT	Construction of SGNHh ClosTron vectors
1060-EBS2	TGAACGCAAGTTTCTAATTTCGGTTAAAAGTCGATAGAGGAAAGTGTCT	
1060-IBS	AAAAAAGCTTATAATTATCCTTACTTTTCCAGTTCGTGCGCCCAGATAGGGTG	
2017-EBS1d	CAGATTGTACAAATGTGGTGATAACAGATAAGTCGTTGCGGGTAACTTACCTTTCTTTGT	
2017-EBS2	TGAACGCAAGTTTCTAATTTCGGTTATTTTCCGATAGAGGAAAGTGTCT	
2017-IBS	AAAAAAGCTTATAATTATCCTTAAAAATCGTTGCGGTGCGCCCAGATAGGGTG	
2395-EBS1d	CAGATTGTACAAATGTGGTGATAACAGATAAGTCAATGCTGTTAACTTACCTTTCTTTGT	
2395-EBS2	TGAACGCAAGTTTCTAATTTCGGTTGATTTCCGATAGAGGAAAGTGTCT	

2395-IBS	AAAAAAGCTTATAATTATCCTTAAAATCCAATGCTGTGCGCCCAGATAGGGTG	
EBSuniv	CGAAATTAGAAACTTGCGTTCAGTAAAC	
RamF	ACGCGTTATATTGATAAAAATAATAATAGTGGG	
RamR	ACGCGTGCGACTCATAGAATTATTTCCTCCCG	
1060intronF	GTGTAAATGCAGGTCC	Control of the intron insertion in the genome (gene inactivation)
1060intronR	GTTGTTGAACTGGTTAC	
2017intronF	CGCTATAAGCTCGTAC	
2017intronR	ACCTAATACACCAGCG	
2395intronF	ATCAGGACTTATTGGAG	
2395intronR	GTAAGCTCCTGGTACAG	
1060SPnodock-pSOS-F	CGTAGGATCCAGAATTTAAAAGGAGGGATTAAAATGAAAAAATCCAATTTTATCAC	
1060SPnodock-pSOS-R	AAGTGGCGCCTCAGTGGTGGTGGTGGTGGTGCATTTCTGCCCATATAGCATCTGCTG	Construction of SGNH overexpression vectors
2017SPnodock-pSOS-F	CGTAGGATCCAGAATTTAAAAGGAGGGATTAAAATGAAAAAACTACTTTTATTTTCTATC	
2017SPnodock-pSOS-R	AAGTGGCGCCTCAGTGGTGGTGGTGGTGGTGCATTTCAGCCCACATAGCTTTTGCTGTTGC	
SOSdir	TCTCGTTCATTATAACCCTC	Control of plasmid presence (SGNHh* overproduction)
Narrev	GTTTCTAGCTCTCACATTCTTG	

2